GRAIN BOUNDARY SEGREGATION AND CONDUCTIVITY IN YTTRIA-STABILIZED ZIRCONIA

Monika Backhaus-Ricoult, Michael Badding and Yves Thibault*
Crystalline Materials Research or Characterization Science*, Science & Technology
Corning Incorporated
Corning NY 14831, USA

ABSTRACT

Grain boundary segregation of Y, Mn, La and Fe in doped and undoped 3YSZ and 8YSZ ceramics is studied by spatially resolved TEM/EELS and impedance spectroscopy. The ceramics are free of second phases and intergranular films. Significant enrichment of di- and trivalent ions is found in an 1-2nm wide grain boundary core; total concentrations of Mn^{2+}, Fe^{2+}, La^{3+} and Y^{3+} reach up to 40cat%. Segregation factors depend on the crystallographic structure of the boundary. Enrichment of di- and trivalent dopants yields a negatively charged grain boundary core. According to EELS line spectra, the O K absorption edge height in the layer adjacent to the grain boundary core is increased; it drops within a few nanometers to the bulk value. O K ELNES also changes within this layer. Evolution in OK edge height and fine structure directly demonstrate the oxygen vacancy depleted space charge layer and its characteristics at 3YSZ grain boundaries. Compared to 3YSZ ceramics, segregation is less pronounced in 8YSZ ceramics.

Inter- and intragranular resistivity of doped and undoped ceramics are measured by impedance spectroscopy in the temperature range of 200-500°C. The oxygen ion bulk conductivity of YSZ ceramics remains unaffected by the dopants. The grain boundary resistance suffers a significant increase in presence of the dopants that can be related to strong interactions between oxygen vacancies and di- and trivalent cations in the grain boundary core and to the lower oxygen vacancy concentration in the space charge layer.

INTRODUCTION

Yttria stabilized zirconia and $(Sr,La)MO_3$ perovskites with M = Mn, Fe, Co, Ni are the present material choices for electrolyte and cathode materials of solid oxide fuel cells (SOFC). Both, cubic 8YSZ and tetragonal 3YSZ are taken into consideration because of their respective advantages. The oxygen ion bulk conductivity in fully stabilized cubic zirconia is by a factor of two higher compared to that of tetragonal 3YSZ[1,2]. Tetragonal 3YSZ, however, has superior strength and thermo-mechanical properties that enable processing of much thinner electrolyte layers[3]. In addition, 3YSZ ceramics exhibit less chemical reactivity with lanthanum strontium manganite than the cubic 8YSZ phase[4]. YSZ electrolyte materials are polycrystalline ceramics. Thus, their oxygen ion conductivity comprises bulk and grain boundary contributions. While the bulk conductivity seems to be a direct function of the level of heterovalent dopants and the associated oxygen vacancy concentration[5], literature data on grain boundary conductivity reveal a broad scattering[1,2] that cannot be easily explained. In addition, the grain boundary resistance is usually two to three orders of magnitude higher than the intragranular resistance.

It shall be recalled that YSZ electrolytes are typically obtained by ceramic processing routes. Even the purest commercial starting powders still contain impurities at the level of 50-100ppm.

Typical impurities are silica, alumina, iron oxide, sodium oxide, hafnium oxide. As a consequence, even purest YSZ ceramic electrolytes have at least this level of impurities.

Low-purity YSZ ceramics usually exhibit much higher impuritiy levels. A high silica content is often responsible for the presence of second phase in the ceramics. Triple points are decorated by glass pockets and grain boundaries are more or less continuously wetted by glass films. Such glassy films constitute a blocking layer for oxygen ion conduction[2]. The very high grain boundary resistance in YSZ ceramics with high silica content can easily be explained on the basis of these observations. In very clean ceramics, no second phases or glassy grain boundary films are found; their grain boundary resistance, however, still remains by a factor of hundred to thousand higher than the intragranular resistance. In the literature, an intrinsic grain boundary blocking effect is suggested[6,7]; it is supported by electrochemical measurements, however, no evidence for such effect is brought by direct microstructural observations.

A grain boundary is the transition zone between two crystals of different orientations with a relaxed structure and energy topography that promote local variations in charge distribution and chemical composition (segregation). As a consequence, at the grain boundary itself and in its proximity, stoichiometry and chemical composition may differ from the bulk crystals. Within the few atomic layers of the "grain boundary core", the chemical composition changes abruptly and evolves then continuously over the more extended space charge layer. Ionic crystals usually contain low concentrations of statistically distributed point defects in the bulk. Segregation of charged defects and species to the grain boundary core creates an electric "core" charge, which, through the coupling with the associated electric field, imposes a redistribution of the charged defects in proximity of the boundary within the so-called space charge layer[8]. The thickness of the space charge layer is on the order of the Debye-Hueckel length. The concentration profiles of the charged species in the layer can be derived from the constancy of the electrochemical potential over the entire ionic crystal, including the space charge layer. Modeling of grain boundaries in yttrium doped zirconia suggests that the enrichment of di- and trivalent dopants in the grain boundary core is associated with a depletion of oxygen vacancies in the space charge layer. Since the dielectric constant of zirconia is small and the heterovalent dopant level in partially or fully stabilized zirconia high, space charge layers are expected to be very narrow. Electrochemical measurements suggest a grain boundary "electrochemical" width of several nanometers; HRTEM crystal structure analysis indicate a "structural" width of 1nm.

Ab initio calculations provide the exact atom and charge distribution for some very special grain boundaries, but the energy topography of the uncountable possible grain boundaries and the atom distribution especially in presence of high dopant concentrations with high segregation factors still remain unaddressed and leave numerous questions on the grain boundary conductivity of YSZ ceramics and their variability.

In order to contribute to the understanding of the grain boundary segregation in YSZ and its influence on the intra- and intergraunlar conductivity, we studied in the present work the grain boundary chemistry in doped and undoped polycrystalline tetragonal 3YSZ and cubic 8YSZ by spatially resolved analytical transmission electron microscopy and electron energy loss spectroscopy, quantified the segregation and used those findings to interpret bulk and grain boundary specific area resistance of those ceramics.

EXPERIMENTAL

YSZ electrolyte layers were processed by slip casting and firing 3YSZ and 8YSZ powders (YSZ with 3 and 8 mol % Y_2O_3 from Tosoh, Japan) to full density at 1430ºC. After firing, 3YSZ

ceramics have a uniform microstructure and a narrow grain size distribution with an average grain size of about 300 nm. According to X-ray diffraction, they are composed of tetragonal phase with negligible amount of monoclinic phase. After long time annealing in air at temperatures between 700ºC and 1300ºC, no significant phase transformation or increase in grain size was observed. At the same firing temperature, 8YSZ ceramics sinter to larger grain size, ranging from 2 to 5 μm. Impurity levels in the ceramics were close to the initial powder quality. Specifications by Tosoh indicate <50ppm Al_2O_3, <20ppm SiO_2, 70ppm Fe_2O_3, 200ppm Na_2O for the powders.

The YSZ ceramics were doped with Mn and La or Fe and La by exposing them at 1250ºC for different durations to (La,Sr)MnO_3 or (La,Sr)FeO_3. The dopant concentrations were determined by microprobe and ICP analysis. Dopant levels in the samples are summarized in Table 1.

Table 1: Global dopant concentrations in studied YSZ ceramics

Sample	wt% Y_2O_3	wt% MnO	wt% FeO	wt% La_2O_3
3YSZ-0	6.5	-	-	-
3YSZ-A	6.5	0.35	-	0.2
3YSZ-B	6.5	0.45	-	0.3
8YSZ-C	18	-	0.5	0.1
8YSZ-0	18	-	-	-
8YSZ-C	18	0.03	-	0.02
8YSZ-C	18	-	0.5	0.1

Bulk and grain boundary resistivity of undoped and doped electrolyte were determined by impedance spectroscopy. For testing, a symmetric two-electrode, four-wire set up was chosen. Identical electrodes of porous LSM/3YSZ were sintered on both sides of the electrolyte and connected via a porous (Ag,Pd)-YSZ layer or a Pt-Au-Pd contact to silver leads. In the entire set up, potential sources of impurities, such as Pt-paste or low purity metal leads were carefully avoided. The used quality of silver was 99.999%; the Pt-Au-Pd quality was lower with Fe (0.2 at%), K (400ppm), Na (150ppm) and Si as main impurities. A well defined nominal active area of 1cm^2 was achieved by a cross printing pattern of the electrodes. The test cells were introduced in a protective alumina tube in a tubular furnace and brought to the test temperature. Impedance data were acquired with a Solartron system (1260 Frequency Response Analyzer/1287 Electrochemical Interface) with no applied bias at temperatures between 200 and 500ºC in air. The frequency was varied from 1 MHz to 100mHz. The amplitude applied between working and reference electrode was 30mV. 10 points per decade of frequency were measured while scanning from the highest to the lowest frequency. Bulk, grain boundary and contact contributions to the impedance were fitted by an equivalent circuit comprising a parallel resistor and constant phase element for each observed arc. Constant phase elements were used in the modeling instead of simple capacitors because they describe better the real system with its depressed arcs.

The local grain boundary chemistry in undoped and doped 3YSZ and 8YSZ electrolyte was studied by spatially resolved transmission electron microscopy (TEM) with energy dispersive analysis (EDX) and electron energy loss spectroscopy (EELS). Sample cross-sections were mechanically polished to an electron transparent wedge and then ion-milled for some minutes to remove the mechanically damaged surface area. In the goal of achieving very high spatial

resolution and resolving the grain boundary chemistry and electronic structure, the VG HB501 STEM13 of the Cornell CCMR facility with its probe size of 0.22 nm was used. It is equipped with a cold field emission gun and operated at 100 kV. A collection semi-angle of the spectrometer of 15mrad, an energy dispersion of 0.3 eV/ch and an emission current of 2.3 pA were the typical operation parameters. The EELS data were acquired by a CCD camera from the Parallel Electron Energy Loss Spectrometer (Gatan PEELS). Spectra of the Sr M, Y M, Zr M, Mn L, Fe L, O K, La L, Si L and Al L characteristic absorption edges were acquired. The evolution of the chemical composition across the grain boundaries was tracked by acquiring line spectra for the different edges while stepping the probe discontinuously across a grain boundary (aligned parallel to the beam). Spectra were explored manually. The characteristic elemental signals were extracted from the spectra by subtracting the background under the characteristic edges under use of a power law fit. Comparison of boundary spectra to those of the adjacent bulk phases was used to identify major changes in composition and in electronic structure at the grain boundaries. Chemical shift and near edge fine structural details were then used to identify in a "finger print"-type analysis valence states and bonding in the grain boundary core. Concentration profiles were corrected for the beam broadening within the foil. Reference spectra of known perovskite compositions were used to quantify the segregation profiles.

Overlap of Y and Zr M absorption edges, broad edges and few characteristic features in the M-edges made it difficult to identify and quantify modifications in the Y, Zr and Sr M edges at the grain boundaries. Only a slight hump at the energy location of the Y $M_{2,3}$ at 300 and 312eV was occasionally noticed when studying 3YSZ ceramics. Even though this feature was more pronounced in 8YSZ ceramics, its separation from the Zr M-edge remained difficult because the edge features change with sample thickness. The same difficulties applied to the Sr-M edge. Therefore, these elements were mainly tracked by EDX in the VG, but with a lower spatial resolution. Spatially resolved study of the Y L, Zr L edges was not possible in the VG501B because the small probe size, 100KV operation voltage did not provide sufficient signal intensity for the >2000eV range.

RESULTS

Mobility of Dopants in 3YSZ and 8YSZ ceramics

Figure 1 illustrates the microstructure of the 3YSZ and 8YSZ ceramics. 3YSZ ceramics exhibit a very homogeneous microstructure with narrow grain size distribution and an average grain size of 320nm, while grain sizes in the 8YSZ ceramic are by a factor ten larger and follow a much broader distribution in size and shape. Grain boundaries typically show little curvature.

Upon exposure to lanthanum strontium manganate or ferrate, lanthanum and manganese or iron dissolved into zirconia and diffused into the ceramic. Overall dopant concentrations are summarized in Table 1.

Bulk diffusion of the cations was found to be rather slow in both, cubic and tetragonal phase. At 1250ºC, interdiffusion coefficients range in the order of 10^{-17}cm^2/s. Grain boundary diffusion is by a factor of 10^6 faster. At 1250ºC, grain boundary interdiffusion coefficients of $D_{gb} = 10^{-10.5}$ cm^2/s for manganese, $D_{gb} = 10^{-10.5}$ cm^2/s for iron and $D_{gb} = 10^{-11.3}$ cm^2/s for lanthanum were determined in 3YSZ. In 8YSZ, grain boundary diffusion coefficients were by a factor of two smaller. Data for bulk and grain boundary diffusion in 8YSZ and 3YSZ ceramics at various temperatures are summarized in Figure 2.

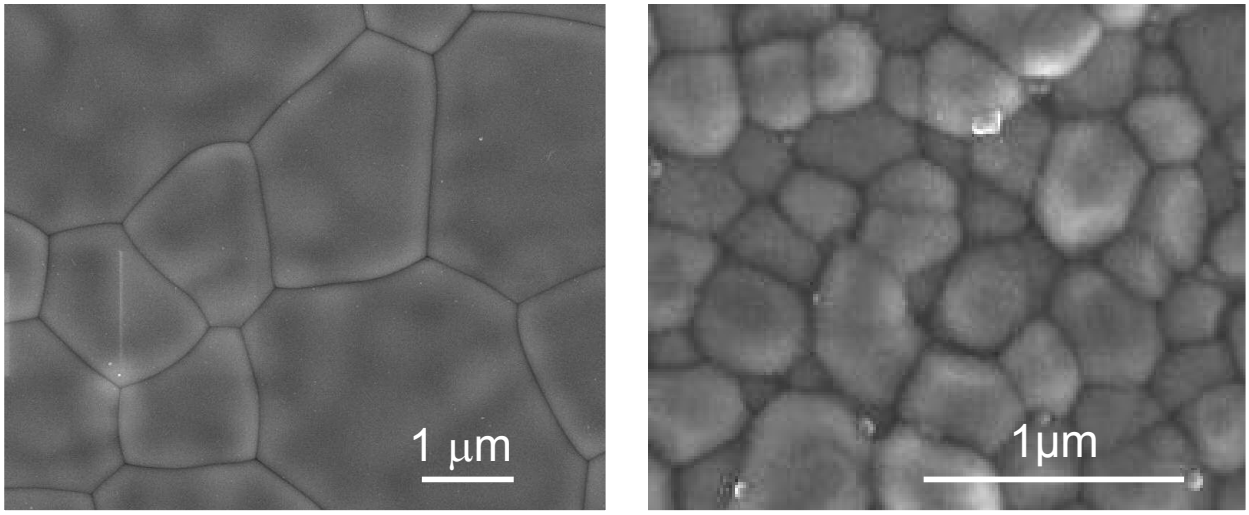

Figure 1: SEM micrographs illustrating the typical microstructure of the 3YSZ and 8YSZ ceramics

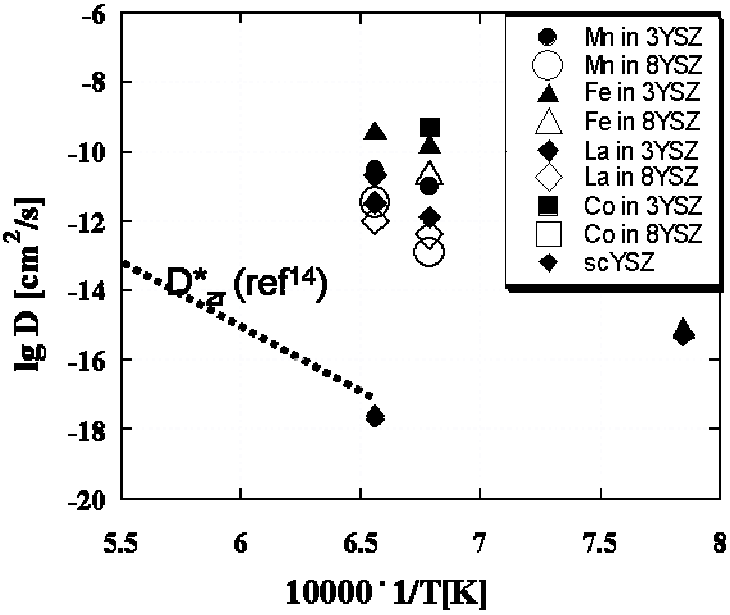

Figure 2: Bulk and grain boundary chemical diffusion coefficients of Mn, Fe, Co, La in 3YSZ, 8YSZ and single crystalline 10YSZ (scYSZ) as a function of temperature

Grain Boundary Chemistry

EDX/TEM analysis of a large number of grain boundaries in the undoped electrolyte revealed significant segregation of yttrium to the grain boundaries. Typical spectra are presented in Figure 3a. The yttrium enrichment varies considerably between grain boundaries, showing that the core chemistry depends on the precise crystallographic structure of the grain boundary. Typically, the segregation factor for yttrium in the 3YSZ ceramic ranged between 2 and 3.5. Triple junctions exhibited slightly higher factors (around 3). Zr and Y M ELNES did not provide any information on changes in bonding.

However, the oxygen edge of the grain boundary core showed characteristic modifications compared to the adjacent bulk grains, Figure 3b. They result from yttrium segregation to the grain boundary core. Firstly, the O K edge height was found to be low in the core, indicating a lower local oxygen content compared to the bulk (low loss spectra did not reveal any change in sample thickness). A possible explanation is the lower atom density in the core region. This change goes hand in hand with a change in the oxygen near edge fine structure. The relative intensity of the peak doublet at 527/531eV is changed, and the doublet peak broadened, suggesting that additional electronic states are involved in the core bonding. Secondly, a more continuous change in oxygen absorption edge height is observed from the grain boundary core towards the bulk. The oxygen absorption edge height is considerably raised in proximity of the core and then drops slowly over several nanometers to the bulk characteristic height. The variation in oxygen absorption edge height can be interpreted in terms of oxygen vacancy concentrations and then indicates a severe depletion in oxygen vacancies in a space charge layer that extends over some nanometers.

The ceramics contain a low level of silica and alumina impurities. Conventional and high resolution TEM analysis did not reveal any discontinuous glass films or triple point glass pockets. However, these impurities could be enriched at grain boundaries. To get further insight in their segregation, the absorption edges of those elements were tracked and monitored while scanning across numerous grain boundaries. Effectively, it was possible to detect by averaging over multiple acquisitions a very weak aluminum signal in the bulk and at the grain boundary.

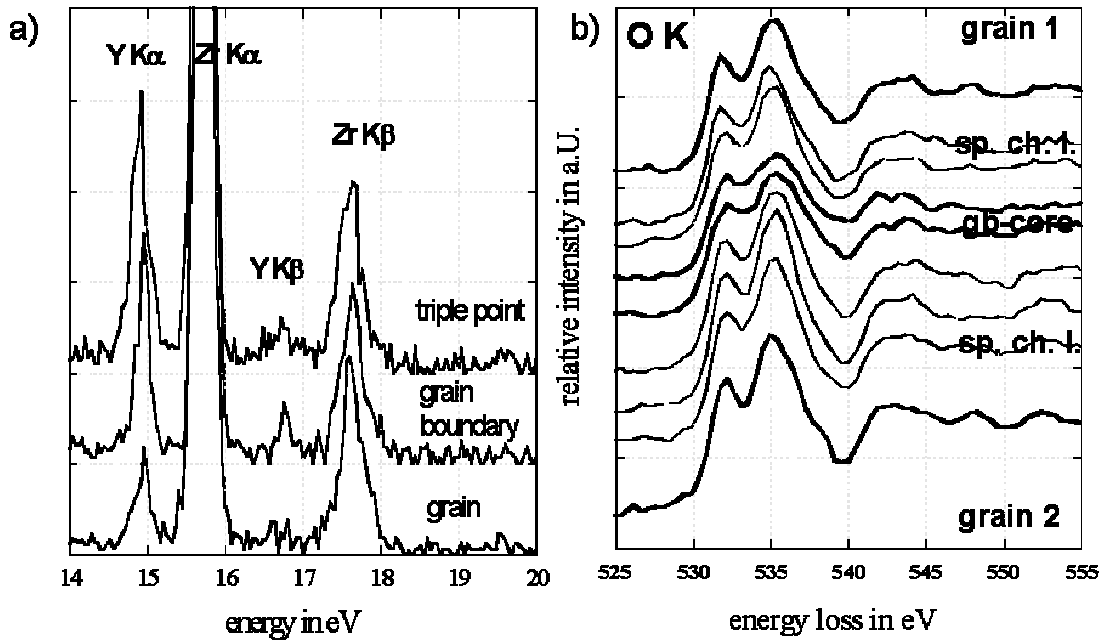

Figure 3: a) Normalized EDX/TEM spectra of the Y K and Zr K peaks at bulk grain, grain boundary and triple point locations in undoped 3YSZ ceramic illustrating the segregation of yttrium to grain boundaries b) O K ELNES line-scan across a grain boundary in the 3YSZ ceramic illustrating the particular fine structure in the core (gb-core) and increased oxygen edge height and doublet intensity ration in the space charge layer (sp.ch.l.). The distance between the subsequent spectra is 2.5nm.

The absolute aluminum concentrations were very small, the enrichment factor at grain boundaries less than 1.5. Within the detection limit of the technique (5-10% of a monolayer), silicon was not observed. The low silicon bulk concentration (confirmed by microprobe analysis) was not accessible by the technique. At grain boundaries, no silicon was detected. It has to be concluded that no significant silicon segregation to grain boundaries occurred in the high purity 3YSZ. Further on, the larger size hafnium ions did not segregate to the boundaries.
Undoped 8YSZ electrolyte showed much less yttrium enrichment of the boundaries.

Doped electrolyte showed significant segregation of the di- and trivalen dopants to its grain boundaries. EDX/TEM spectra revealed the presence of Mn, La, Fe at the grain boundaries, and did not show any signal for these elements in the adjacent bulk grains. EELS/STEM investigations provided details on the grain boundary core composition. Effectively, high local concentrations of manganese and or iron and lanthanum were detected in the grain boundary core. Segregations was found to be more important for grain boundaries of 3YSZ ceramics; 8YSZ ceramics showed more pronounced solubility of the dopants in the bulk grains and only a small enrichment compared to those bulk concentrations. 3YSZ ceramics exhibited negligible concentrations of the dopants in the bulk and grain boundary core concentrations in the order of 20-30%. The segregation factor reached several orders of magnitude!

Figure 4 shows the absorption edges of manganese, lanthanum and oxygen in the grain boundary core and in the adjacent grains of a doped 3YSZ ceramic. Within the detection limit of the EELS technique, no manganese or lanthanum was found within the 3YSZ grains. At the grain boundary, in contrast, strong signals of manganese (Mn $L_{2,3}$ at 640eV) and lanthanum (La $M_{4,5}$ at 840eV) were visible, Figure 4. In addition, the oxygen signal at the grain boundary was again modified: In the grain boundary core, a change in the relative peak intensities of the doublet at 536eV reveal a strongly defective zirconia. In the layer adjacent to the core, the doublet exhibits a changed intensity with a high second peak, characteristic for YSZ with low dopant levels and thus low oxygen vacancy concentrations. The oxygen absorption edge height evolves over several nanometers before stabilizing on the bulk value.

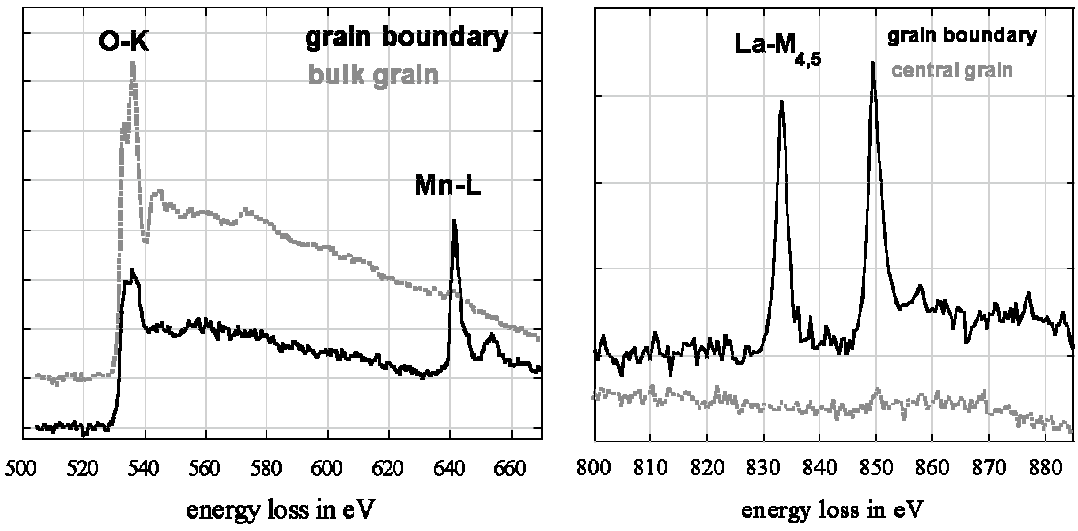

Figure 4: Absorption edges of oxygen, manganese and lanthanum in a bulk 3YSZ (black) grain and on the grain boundary core (dotted grey) in the 3YSZ-A ceramic

Numerous grain boundaries have been studied in samples with different dopant levels after their annealing in air at 1250°C. No modifications compared to the bulk were observed in the Zr M, Y M and Sr M edges; however, it shall be recalled that these M edges are not very sensitive to local bonding details and that minor changes may not have been identified. For manganese, iron and lanthanum, the height of the characteristic absorption edges evolves across the grain boundaries as demonstrated in Figures 5 and 6. A steep intensity profile was found with a maximum in the grain boundary core. The entire profile never extended over more than 2-3nm. The absorption edge height was quantified under use of the reference materials (La,Sr)MnO_3 and (La,Sr)FeO_3. Concentration profiles were deduced from the line spectra. The maximum concentration varied from grain boundary to grain boundary, reflecting a dependency on the precise crystallographic nature of the grain boundary. For manganese, the maximum concentrations varied between 10 and 25cat%, for lanthanum, 9-12cat%. The profiles were rarely symmetric, thus accounting for the crystallographic asymmetry of the boundaries.

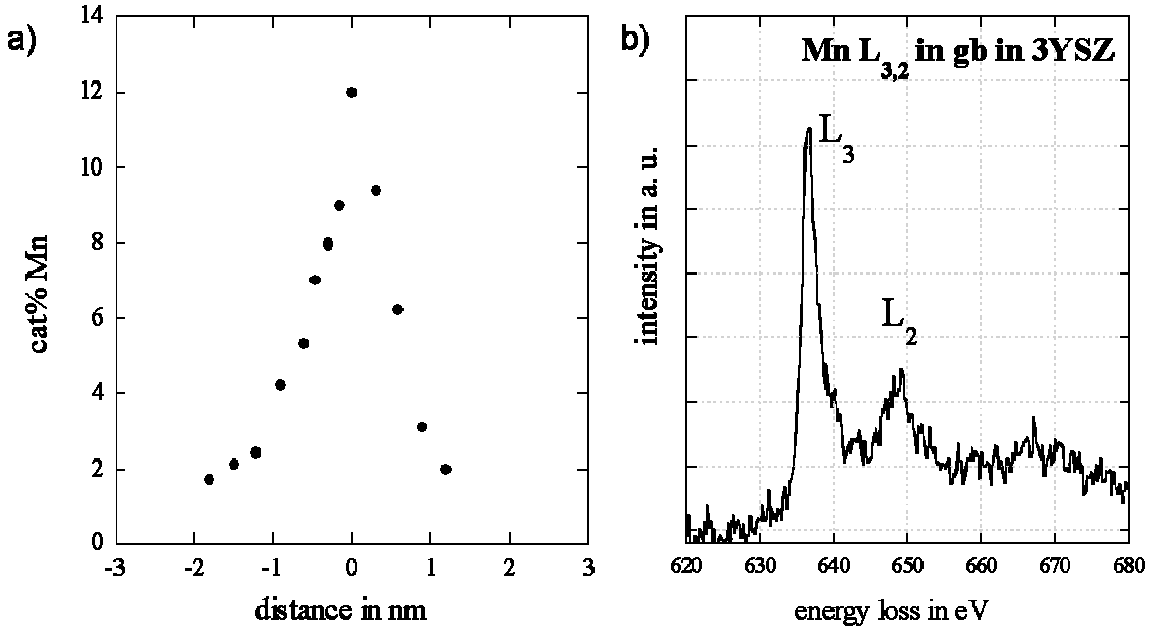

Figure 5: a) Series of manganese absorption edges acquired while crossing a with an interstep of 0.3nm, a) manganese concentration profile at a 3YSZ-A grain boundary obtained from Mn -scan across a grain boundary (position 0 nm), b) ELNES fine structure of the manganese absorption edge in the grain boundary core

The manganese valence state was determined from the $L_{2,3}$ chemical shift and the L_3/L_2 ratio. According to the literature, the L_3/L_2 white line ratios change from 5 for Mn^{4+} to 4.7 for Mn^{3+} to 3.4 for Mn^{2+} [9]. Manganese in the grain boundary core of 3YSZ, see Figure 5b, demonstrated a L_3/L_2 ratio of about 3, thus clearly indicating that the oxidation state of manganese in the grain boundary core was 2+. Energy location and energy split confirmed this statement.

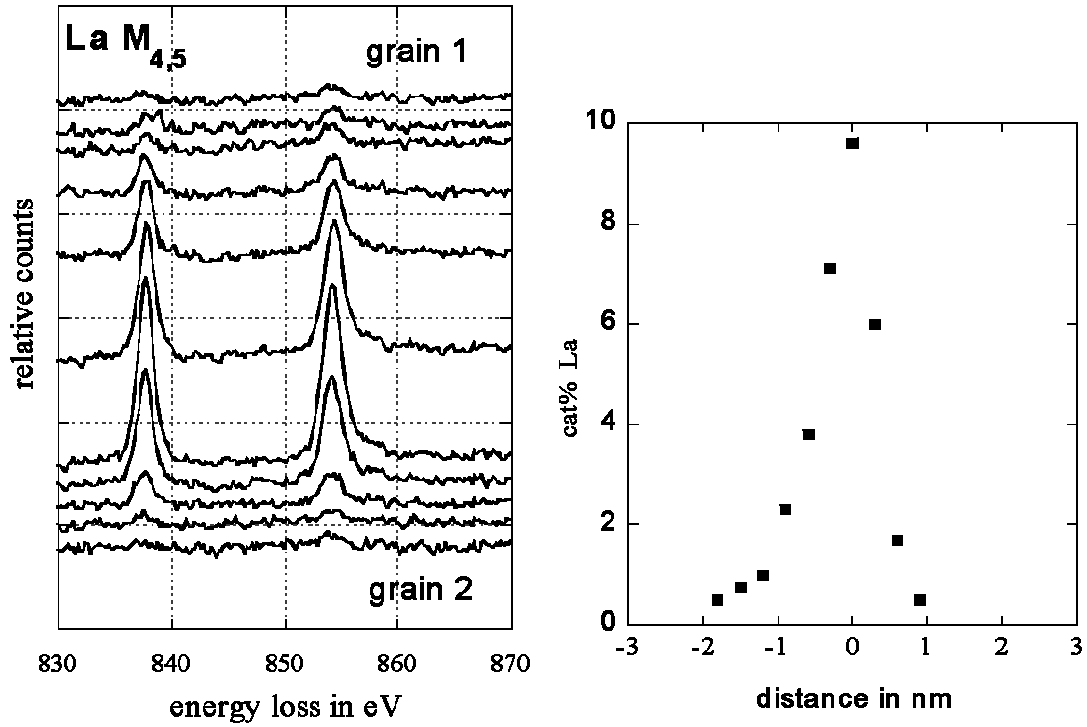

Figure 6: a) Series of lanthanum absorption edges acquired while crossing a grain boundary in 3YSZ-A with an interstep of 0.3nm ; b) corresponding concentration profile of lanthanum across the grain boundary

Oxygen scans across the grain boundaries showed typically a decrease in absorption edge height of about 20% in the core as demonstrated in Figure 7. This corresponds well to a Mn^{2+} and La^{3+}-rich grain boundary core. For the core absorption edge, in addition, a change in the near edge fine structure was observed. The peak intensity was increased at higher energies, yielding a high energy shoulder of the second peak of the doublet and an increased intensity in the doublet valley. Heavily doped defective zirconia in fluorite structure and pyrochlore usually show such a symmetric doublet; it can be speculated that a doublet with equal peak intensities might be related to oxygen vacancy ordering and deformation in the next neighbor symmetry. The high energy shoulder seems to be related to Mn-O-bonding.

Impedance Results

Typical impedance spectra for undoped and doped 3YSZ and 8YSZ ceramics are presented in Figure 9. The impedance spectra are composed of three arcs, a low frequency arc representing the bulk conductivity, an intermediate frequency arc representing the grain boundary resistivity and a more or less visible high frequency arc that originates from the resistance of the two electrolyte/electrode contacts. Comparison of the low frequency arcs of undoped and doped 3YSZ ceramics shows that the intragranular resistance does not significantly differ. The same is valid for 8YSZ ceramics. However, bulk conductivities of 3YSZ and 8YSZ are different. The impedance curves are fitted by an equivalent circuit. The area specific resistance for the bulk R_g is computed from $\rho_g = R_g \times S/h$ with S being the measured area, h the

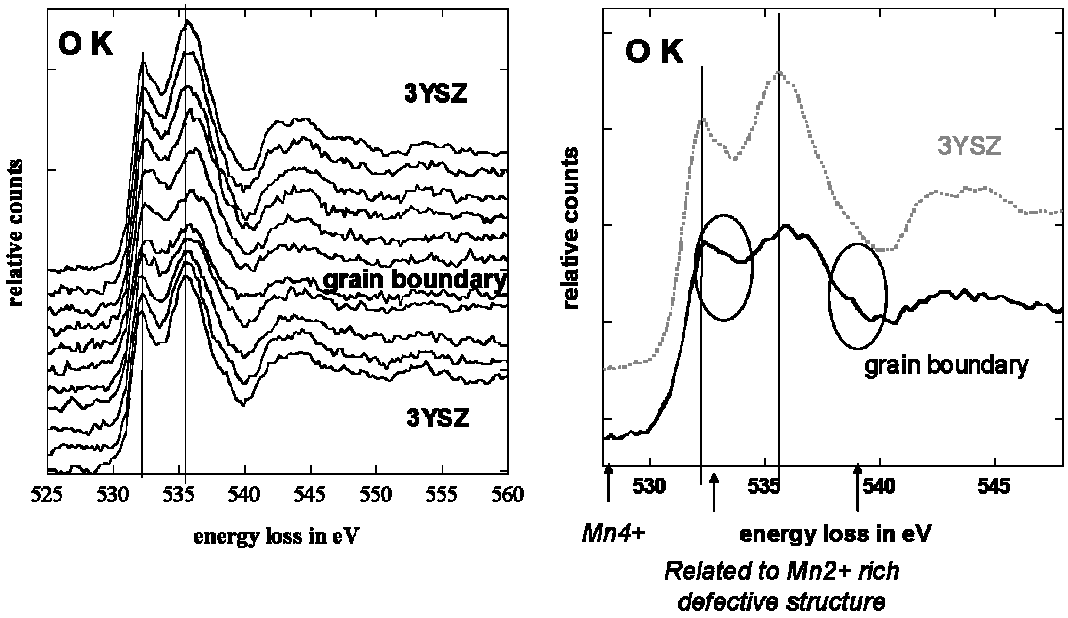

Figure 7: Series of O K absorption edges acquired while crossing a grain boundary in 3YSZ-A with 0.3nm as interstep; details of O K ELNES in bulk and grain boundary core

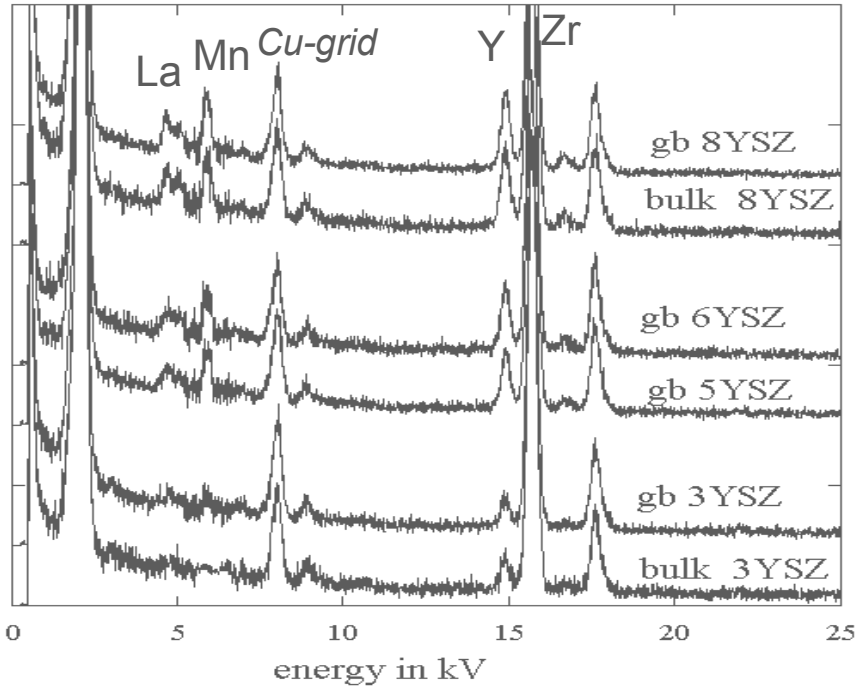

Fig. 8: Bulk and grain boundary EDX spectra in Mn/La-doped ceramics with different Y-content

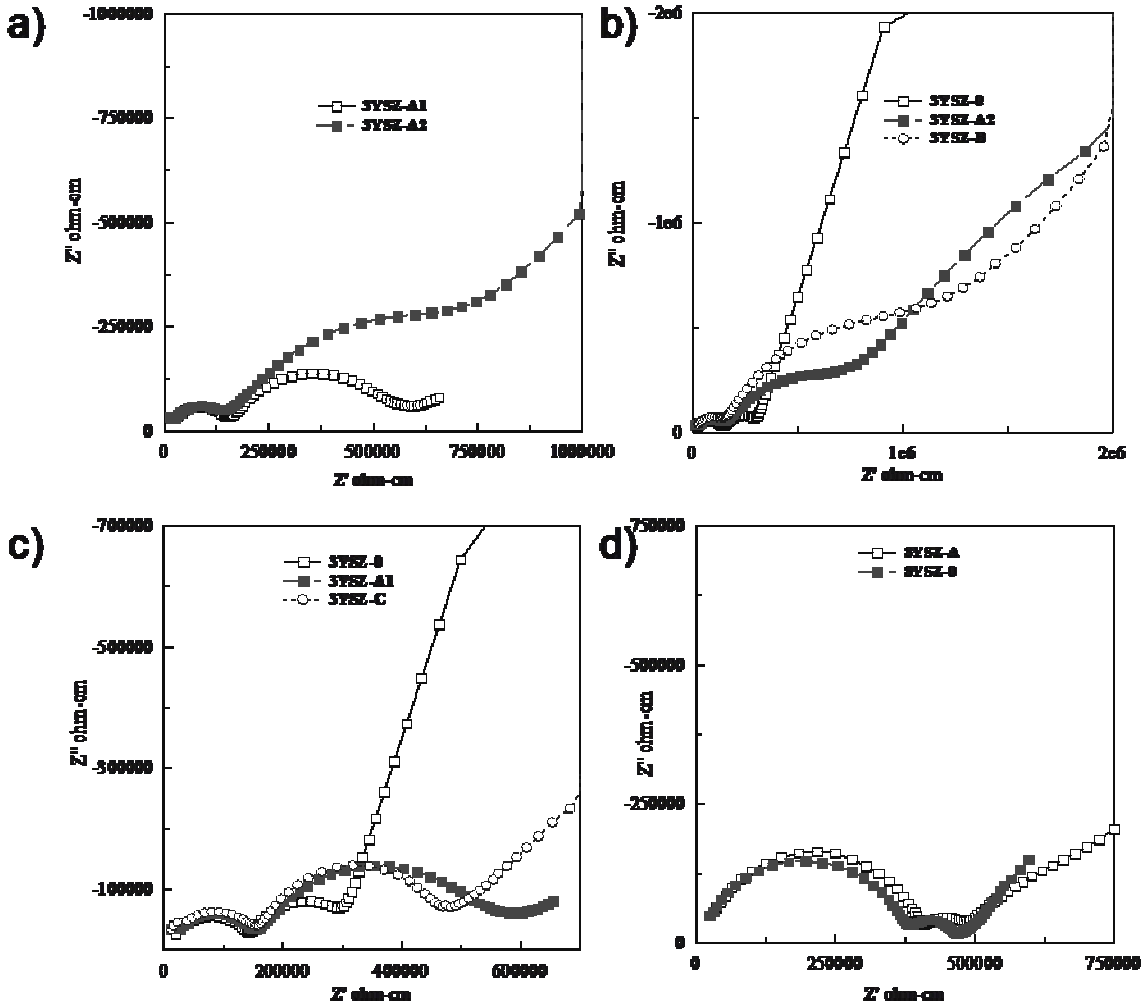

Figure 9. Typical impedance spectra of doped and undoped 3YSZ ceramic at 300ºC: (a) comparison of 3YSZ electrolytes with different La/Mn-concentrations; (b) comparison of Mn/La- and Fe/La- doped 3YSZ; (c) effect of contact paste. Samples are identified in Table 3.

electrolyte thickness (typically 20 µm for 3YSZ and 40 µm for 8YSZ ceramics). For pure 3YSZ at 300°C, a grain resistance of 147 kΩcm is obtained, for pure 8YSZ 386 kΩcm. Results of the activation energies are summarized in Table 3.

The second arc of the impedance spectra strongly changes with doping. Figure 9a demonstrates how the grain boundary impedance changes with dopant concentration. The grain boundary area specific resistance is derived from $\rho_{gb} = R_{gb} \times S_{gb}/n\ \delta_{gb}$ with δ_{gb} being the grain boundary core width, n the number of grain boundaries in the foil. Resistance data for bulk and grain boundaries are presented for a wide temperature range in Figure 10.

For high purity materials, bulk and grain boundary resistance are of similar size. For 3YSZ materials, for temperatures below 300ºC, usually the grain boundary resistance is smaller, for temperatures above 300ºC, it is inversed. Highly doped ceramics like 3YSZ-B exhibit a dramatic increase in grain boundary resistance compared to the undoped material by a factor of 50 or

larger. For 3YSZ-A1 and 3YSZ-C, no difference is noticed even though the overall concentration of iron and lanthanum in 3YSZ-A1 is higher than the manganese and lanthanum concentration in 3YSZ-C. This observation has to be explained either to a higher valence state of iron in the grain boundary core than manganese or to differences in stability of the oxygen vacancy-cation pairs of manganese and iron. Since our EELS studies did not reveal significant differences in valence state, the letter explanation seems to apply. For 8YSZ ceramics, the grain boundary resistance is only little affected by dopants. This was expected based on the grain boundary core compositions in 8YSZS ceramics

Table 3: Activation energies for grain and grain boundary resistance in the YSZ materials

Sample	contact	E_A grain in eV	E_A gb in eV
3YSZ-0	Pt-Au-Pd	0.95	1.08
3YSZ-A1	Ag-Pd	0.90	1.19
3YSZ-A2	Pt-Au-Pd	0.91	1.10
3YSZ-	Pt-Au-Pd	0.92	0.96
3YSZ-C	Ag-Pd	0.92	1.12
8YSZ-0	Ag-Pd	1.14	1.25
8YSZ-A	Ag-Pd	1.09	1.2

DISCUSSION

Yttria-stabilized zirconia is an oxygen ion conductor with conductivities in the order of 2 10^{-2} Scm^{-1} and 28 10^{-2} Scm^{-1} at 1000°C for cubic 8YSZ and tetragonal 3YSZ, respectively. Cation diffusion is orders of magnitude slower[10,11,12] than oxygen ion diffusion. According to the literature[13], Zr* tracer diffusion is by a factor 10 faster in 3YSZ compared to 10YSZ with absolute values around $10^{-17}cm^2/s$ at 1200ºC[14]. Diffusion of other dopant cations in YSZ scales with their cation radius; lanthanide cations, Mg^{2+}, Ca^{2+}, Mn^{2+} and Ti show mobilities that are by a factor 3-7 higher than the Zr mobility [15,16,17,18].

During SOFC processing, after few hours of exposure to the cathode materials at 1200-1300ºC, diffusion of manganese into the YSZ electrolyte was noticed and reported in the literature. We determined interdiffusion coefficients in LSM/YSZ and LSF/YSZ couples as a function of Y-level and temperature and distinguished bulk and grain boundary diffusion[19]. Bulk diffusion coefficients are in the order of $10^{-17}cm^2/s$ at 1250ºC. Grain boundary diffusion is faster by a factor of 10^6. Both, bulk and grain boundary cation chemical diffusivities are by a factor ten faster in 3YSZ than in 8YSZ. High activation energies for both, bulk and grain boundary diffusion, yield a steep diffusion onset with temperature. Thus, considerable bulk concentrations of dopants or pollutants are obtained by diffusion only at temperatures above 1400°C. Grain boundary diffusion in 8YSZ and 3YSZ ceramics is already activated at temperatures as low as 1200°C and is responsible for fast doping of grain boundaries at such low temperatures.

It is generally agreed that di- and trivalent dopants introduce oxygen vacancies in the zirconia crystal lattice according to

$$M_2O_3 = 2M'_{Zr} + 3O^x_O + V_O \quad \text{and} \quad MeO = Me''_{Zr} + O^x_O + V_O$$

Fully stabilized zirconia adopts a deformed fluorite structure and requires for its stabilization about 7cat% oxygen vacancies. Partially stabilized zirconia is a two phase mixture

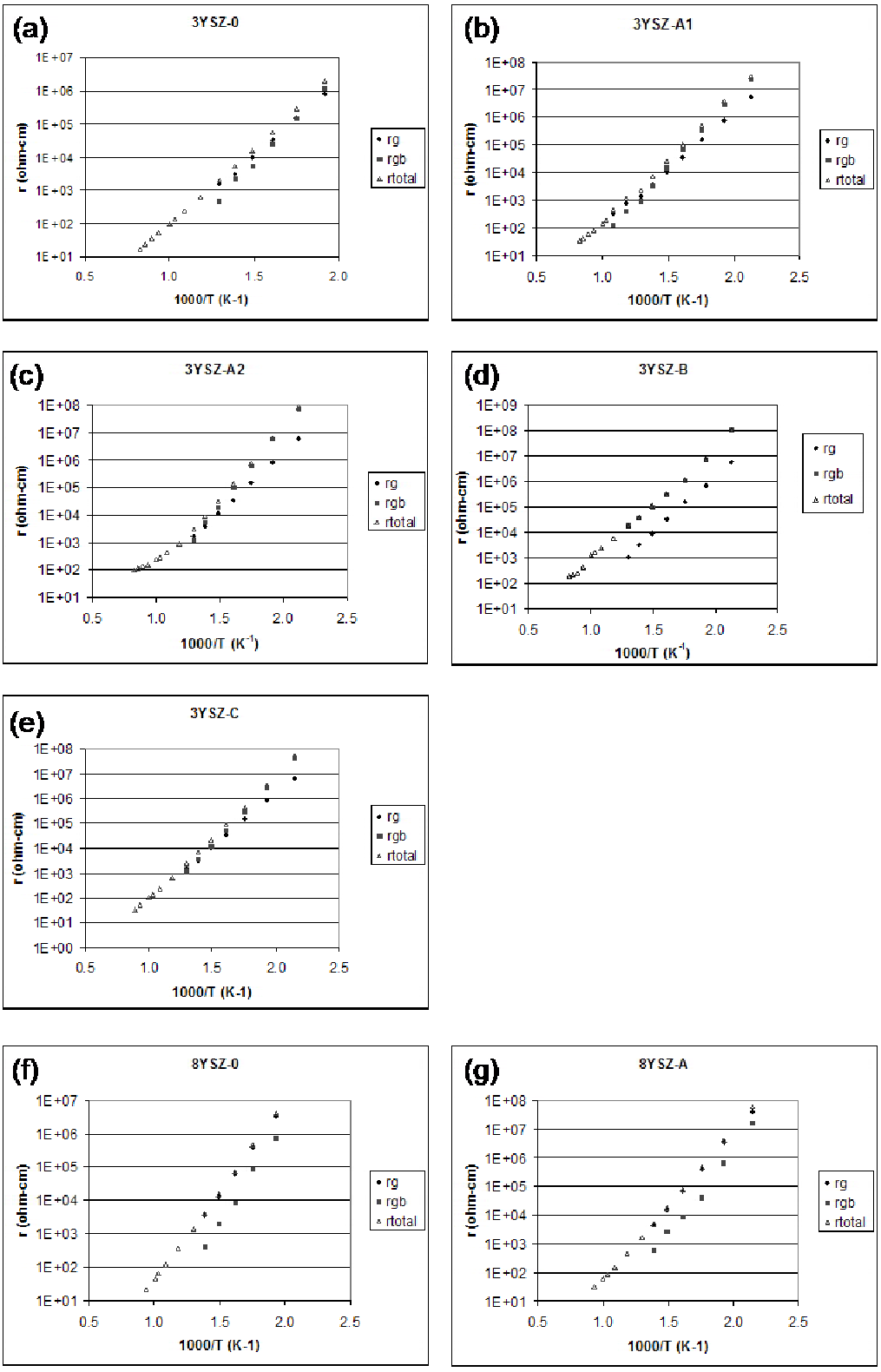

Figure 10. Arrhenius plots for grain and grain boundary resistance for YSZ ceramics as identified in Table 3.

of cubic zironia with precipitates of tetragonal phase, which provide high fracture toughness by the martensitic transformation that they undergo under volume increase in the crack tip stress field. It was demonstrated that single phase very fine-grained tetragonal zirconia exhibits similar properties as partially stabilized zirconia[3]. In bulk zirconia, the oxygen vacancy concentration increases with the dopant level, yielding the well-known relationship between dopant concentration and conductivity for the low dopant concentration range

$$\sigma = \text{const./T } [V_O^{\cdot\cdot}] ([V_O^{\cdot\cdot}]^{-1}) \, e^{-EA/RT}$$

with R being the gas constant, T the temperature, EA the activation energy[20]. For high dopant concentrations, interactions between the defects introduce deviations from the ideal behavior. Usually the formation of defect pairs of type $\{Y_{Zr}'V_O^{\cdot\cdot}\}^{\cdot}$ is considered, but larger defect associates have also been suggested.

Two- and trivalent dopants segregate to the grain boundary core due to charge and size effects. Dopant and yttrium cations are mobile at temperatures above 1200ºC in YSZ; at lower temperature, the dopant concentration profiles are frozen and only oxygen ions and anionic defects equilibrate. For the present case of zirconia, the space charge theory[6] predicts an extremely thin space charge layer due to high dopant concentrations (7-20cat%) and the value of the dielectric constant of around 60.

Assuming that Mn^{2+} La^{3+}, Fe^{2+} and Y^{3+} are the dominating dopant species in the zirconia solid solution, the defect chemistry of the solid solution $(Zr,Y,Mn,La,Fe)O_2$ can be described by the following equations:

$$[VO^{\cdot\cdot}] = \tfrac{1}{2} [Y_{zr}'] + \tfrac{1}{2} [La_{zr}'] + [Mn_{zr}''] + [Fe_{zr}'']$$

Di- and trivalent dopants segregate to the grain boundary because of their charge and size; dominant driving force is the elastic energy gain. Segregation produces a local negative charge in the core and stabilizes cation vacancy and oxygen vacancy concentrations in the adjacent areas of the grains at levels different from the bulk equilibrium concentrations. The Boltzmann-Poisson equation indicates the evolution of their concentrations. Calculations of the defect concentrations in the space charge layer have been realized by Guo and Maier [6].

At the high dopant levels of 3YSZ or 8YSZ, the space charge layer shows a depletion in oxygen vacancies (cation vacancy concentrations are negligible in the bulk and in the space charge layer). Absolute oxygen vacancy concentrations and width of the space charge layer depend on the dopant concentration. In 8YSZ, the bulk oxygen vacancy concentration is around 20%. In the space charge layer close to the interface, the oxygen vacancy concentration is dropped to almost zero, but raises rapidly within a few atomic layers to almost the bulk value. In 3YSZ, the bulk oxygen vacancy concentration is smaller and the oxygen vacancy depletion close to the interface extends slightly further into the bulk. Ou experimental observations suggest an extension of the space charge layer over 3-5nm.

In a simplified vision, the grain boundary can be described by a set of double layers with a heavily substituted negatively charged core and its surrounding severely oxygen vacancy depleted space charge layers. All three layers have to be considered as blocking for oxygen ion transport due to the strong interaction of di- and trivalent cations in the core with the oxygen vacancies and due to the severe depletion in oxygen vacancies in the space charge layers. For simplified impedance modeling, grain boundaries can be described as a single layer with very low oxygen ion conductivity.

Grain Boundary Chemistry In Undoped YSZ Ceramics

Due to its sensitivity to the local environment of the oxygen atom in the zirconia polymorphs, O K ELNES differs for cubic, tetragonal and monoclinic phase[21] and allows to distinguish the phases by the respective peak intensities of the doublet at 535eV. Several spatially resolved studies by TEM/EDX or TEM/EELS of grain boundaries in cubic and tetragonal zirconia are reported. In pure materials, yttrium is found to be enriched at grain boundaries. Segregation factors of up to 4 are reported in 3YSZ [22] (densified at 1450ºC), and of 1.5 for 8YSZ [22]. These findings are in agreement with our observations of pure YSZ ceramics. We found a similarly small enrichment in 8YSZ boundaries (factor 1.2-1.6) and a larger enrichment in 3YSZ boundaries (factor 2-3.5). In the above mentioned literature, no modification in O K ELNES was noticed. This could be related to missing spatial resolution. We observed for 3YSZ grain boundaries a systematic evolution of the intensity ratio in the peak doublet at 535eV across the boundary with an increased peak intensity ratio at the boundary that evolved within a few nanometers into the typical 3YSZ bulk ratio. In terms of oxygen vacancy concentrations, our observation relates to the oxygen vacancy depleted space charge layer with its high depletion at the boundary that disappears over 3-5nm towards the bulk. In addition, we observed a drastic change of the OK ELNES in the grain boundary core; core OK ELNES exhibits the feature of highly doped defective cubic zirconia. This is not surprising. The core composition is 10YSZ or even more Y-rich.

For grain boundaries in undoped 8YSZ, we did not notice significant changes in O K ELNES at the grain boundary.

Grain Boundary Chemistry in Doped YSZ Ceramics

It is reported in the literature that yttrium segregation is easily suppressed in presence of other dopants such as aluminum. From our study of doped YSZ ceramics, we confirm that yttrium easily grain boundary core sites to other dopants. Manganese, lanthanum and iron are present at much lower overall concentrations in our 3YSZ ceramic, but segregate heavily to the grain boundaries because of their larger strain and charge effects. Boundary cores in 3YSZ exhibit extremely high concentrations of di- and trivalent cations, for example 18cat% Mn, 12cat% La and 7cat% Y. Such compositions are close to the bulk stability limit for cubic zirconia! Corresponding to the local environment of oxygen atoms in the grain boundary core, we detected in the grain boundary core O K ELNES features that match highly doped defective cubic zirconia with its height-equivalent O K doublet. Additional high and low energy shoulders in the core O K ELNES indicate the presence of electronic states that imply more direct binding contributions between Mn^{2+} and oxygen.

Grain Boundary Chemistry And Conductivity

Our impedance measurements indicate that the bulk oxygen ion conductivity is little affected by the presence of the dopants. This is not further surprising since almost the entity of the Mn, La, Fe dopants is segregated to the grain boundary and the grain composition is only determined by the yttrium level. The yttrium concentration determines the bulk conductivity; as clearly shown by the differences between 3YSZ and 8YSZ ceramics.

The grain boundary resistance in YSZ ceramics increases with the overall concentration of di- and trivalent dopants and thus with the local segregant concentration in the grain boundary core. If we consider grain boundary core compositions as determined by EELS of 18cat% Mn, 12cat% La and 7cat% Y, a core diameter of 2nm and an oxygen vacancy depleted space charge layer of

about 5nm width, we can simulate the doped YSZ ceramic by a brick model with a brick interior of bulk YSZ conductivity and walls that should represent the three regions of the space charge layer (space charge layer with very low oxygen vacancy concentration, a heavily doped layer of defective fluorite layer and a second space charge layer).

Influence Of Impurities

The studies by Badval et al.[1] of various 3YSZ ceramics illustrate that the bulk conductivity is rather independent of small variations in powder purity. Large variations in grain boundary conductivity, however, leave room for speculations. Our extended studies on impurity segregation in YSZ ceramics suggest that the impurity level in a ceramic in general first decreases with firing temperature (loss of alkali and volatile impurities) and then increases during further firing with temperature and time due to the pick up of impurities by the ceramic from surrounding tube, holder and furnace materials. Thus we found that electrolyte in contact with silica-containing supports enriches in silica. For an overall average of 50ppm silicon or smaller and simultaneous presence of alumina, no glassy grain boundary films or second phase triple point pockets form. At high levels of silica, however, we observed the formation of silicate triple phase pockets and extended glassy films.

High temperature processing, firing of electrodes or contacts or long time impedance testing with electrodes and leads always implies the danger of introducing pollutants that are mobile in the grain boundaries. On a first view, platinum seems to be an inert material, ideal for contacting a clean electrolyte; however, ICP analysis of various batches and origins of Pt-paste showed that Pt-paste usually contains considerable amounts of silica, iron, calcium….. All these elements are present in small quantities in Pt-leads and -electrode contacts; they are mobile according to our diffusion studies and arrive with time during firing and electrochemical testing in the electrolyte and distribute in its grain boundaries or segregate to interfaces and surfaces[23]. Thus data obtained with Pt-paste contacts have to be carefully analysed; especially an evolution of conductivity with time is often related to pollution of the system from outer sources.

We illustrated in our work an impurity induced change in grain boundary conductivity for the doped 3YSZ electrolyte. The Pd-Au-Pt electrical contacts contained 0.2 at% iron, 400ppm K and 150ppm Na and silicon as main impurities. Iron was mobile at the firing temperature of the contact, diffused into the electrolyte and segregated to the grain boundaries. As a result, the grain boundary conductivity dropped significantly compared to electrolyte that were tested with (clean) Ag-Pd contacts, Figure 9c. The change in activation energy, Figure 10, indicates that other impurities besides iron have participated in the modification of the grain boundary chemistry..

CONCLUSIONS

In Mn, La and Fe-doped and undoped high purity 3YSZ and 8YSZ ceramics, spatially resolved TEM/EELS and impedance spectroscopy have been used to study the grain boundary segregation. All boundaries exhibit segregation. In undoped materials, yttrium segregates to the boundaries with enrichment factors of 2-3.5 in 3YSZ and 1.2-1.6 in 8YSZ. Significant enrichment of di- and trivalent ions occurs in doped materials. The enrichment of the cations is usually restricted to a grain boundary core of 1-2nm in width. Total concentrations of Mn^{2+}, Fe^{2+}, La^{3+} and Y^{3+} in the core can reach up to 40cat% in 3YSZ ceramics; in 8YSZ ceramics, those

concentrations are by a factor of two to three lower. The reason for this difference may be the higher bulk solubility of the cations in 8YSZ and a lower coordination number in the cubic phase. Segregation factors were found to depend on the crystallographic structure of the boundary. O K ELNES features in the core are different from the bulk and suggest a highly defective fluorite-type bonding in the core.

The grain boundary core enrichment with lower valent dopants imposes a negative charge on the grain boundary core. EELS of undoped 3YSZ revealed that the O K absorption edge height is increased in the region adjacent to the grain boundary core; it drops within 3-5nm distance to the bulk value. O K ELNES changes within this layer, exhibiting close to the core the features of tetragonal YSZ with very low dopant levels. The evolution in O K edge height and fine structure directly matches an oxygen vacancy depleted space charge layer and is considered as a direct observation of the latter.

Compared to 3YSZ ceramics, segregation is less pronounced in 8YSZ ceramics. O K does not reveal any significant modifications.

Inter- and intragranular resistance of doped and undoped ceramics has been deduced from impedance measurements. It is found that the oxygen ion bulk conductivity of YSZ ceramics remained unaffected by the dopants. The grain boundary resistance was significantly increased by di- and trivalent dopants. This was expected from the grain boundary chemistry. Both, formation of stable defect associates between oxygen vacancies and di- and trivalent cations in the grain boundary core and depletion in oxygen vacancies in the space charge layer contribute to the grain boundary resistance.

ACKNOWLEDGEMENTS

This work made use of the ultra-high vacuum scanning transmission electron microscopy and microscopy facilities of the Cornell Center for Materials Research (CCMR) with support from the National Science Foundation Materials Research and Engineering Centers (MRSEC) program (DMR-0079992). The authors want to especially thank M. Thomas, CCMR, for his support during the STEM measurements. They further want to thank K.Work, M.Carson and J.Brown, Corning Incorporated, for their technical contributions.

REFERENCES

[1] S.P.Badwal, F.T.Ciacchi; Ionics 6,1 (2005)
2 S.P.Badwal, Solid State Ionics 76, 67-80 (1995)
3 M.Ruehle, N.Claussen, A.Heuer; Advances in ceramics Vol.12, p.352 (1984)
4 M.Backhaus-Ricoult, M.Badding, J.Brown, M.Carson, E.Sanford, Y.Thibault; Ceramic transactions 2AM-S8-55 (2004)
[5] High temperature solid oxide fuel cells, ed. Singhal, S.C., Kendall, K., Elsevier, Oxford, 2004
[6] X.Guo, J.Maier; J. Electrochem. Soc 148, E121-126 (2001)
[7] X.Guo, Solid State Ionics, 96, 247-254 (1997)
[8] J.Maier; Prog. Solid St. Chem. 23, 171-263 (1995)
[9] Electron Energy Loss Spectroscopy, R.F. Egerton, Plenum Press NY 1989
[10] F.R.Chien, A.H.Heuer, Phil. Mag. A73, 681 (1996)
[11] H.Solmon, PhD thesis, CNRS- Labo. Phys. Mat. (1992)
[12] S.Weber et al. Applied Surface Science 203/204, 656 (2003)

[13] M.Kilo, M.Weller, G.Borchardt, B.Damson, S.Weber, S.Scherrer, Defect and Diffusion Forum 194-199, 1039 (2001)
[14] M.Kilo et al, J. Applied Physics 94, 7547 (2003)
[15] M.Kilo et al. Journal of chemical physics 121, 5482 (2004)
[16] C.T.Bak et al, J. Am. Ceram. Soc 85, 2244 (2000)
[17] K.Kovalsli, A.Bernasik, A.Sadovski, J. Eur. Ceram. Soc. 20, 951 and 2095 (2000)]
[18] M.Kilo et al. Journal of chemical physics 121, 5482 (2004)
[19] M.Backhaus-Ricoult, Y.Thibault; unpublished
[20] "Solid oxide fuel cells" by S.C. Singhal and K.KendallElsevier, Oxford (2003)
[21] I.M.Ross, W.M.Rainford, A.J.Scott, A.P.Brown, R.Brydson, D.W. McComb, ECERS 24, 2023-2029 (2004)
[22] E.C.Dickey, X.Fan, S.J.Penneycook, JACS 84, 1361-1368 (2001)
[23] M.Backhaus-Ricoult, M.-F.Trichet; Sol. St. Ionics, 150, 143 (2002)